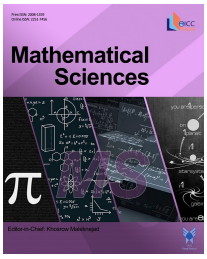

Math. Sci. 2026; 20(1): 19-29

Mathematical Sciences (MS)

https://doi.org/10.57647/mathsci.2026.46781

Research Article

Effect of Rotation on Wave Propagation in Micro-elongated Thermo-elastic Media with Fractional Conformable Derivative under the Refined Dual-Phase-Lag Model

Ahmed Ramady [1,2], Mohamed F. Ismail [3], Hamdy M. Ahmed [4], Soliman Alkhatib [5], Elsaid M. Ramadan [6,*] Eslam Nabil Shawki El-Ganzoury [7]

[1]*GRC Department, The Applied College, King Abdulaziz University, Jeddah, 21589, Saudi Arabia*
[2]*Department of Mathematics and Computer Science, Faculty of Science, Beni-Suef University, Beni-Suef, Egypt*
[3]*Department of Computer Science, Faculty of Computers and Information Systems, Egyptian Chinese University, Cairo, Egypt*
[4]*Department of Physics and Engineering Mathematics, Higher Institute of Engineering, El Shorouk Academy, Cairo, Egypt*
[5]*College of Engineering and Technology (CET), American University in the Emirates (AUE), Dubai intel Academic City, P.O. Box 503000, Dubai, UAE*
[6]*Department of Mathematics, Faculty of Science, Islamic University of Madinah, Medina, Saudi Arabia*
[7]*Department of Physics and Engineering Mathematics, Faculty of Engineering, Ain Shams University, Cairo, Egypt*

[*]**Corresponding author:** m.elsaid@iu.edu.sa

Article History
Received:
25 November 2025
Revised:
7 January 2026
Accepted:
27 January 2026
Published online:
25 March 2026
Published in Issue:
25 March 2026

Abstract:

This study investigates the impact of rotation on wave propagation within a micro-elongated thermo-elastic medium, employing the fractional conformable derivative under Lord-Shulman (L-S) theory, the Dual-Phase-Lag (DPL) model, and the Refined Dual-Phase-Lag (RDPL) model. The governing equations for heat conduction, mechanical motion, and micro-elongation are formulated to account for finite thermal wave speeds and microstructural effects.

By applying non-dimensionalization and normal mode analysis, the coupled system is transformed into analytically solvable form. Explicit solutions for displacement, temperature, stress, and micro-elongation fields are obtained. Numerical results compare L-S, DPL, and RDPL models with and without rotation, and assess the effect of fractional order.

The results show that rotation significantly influences wave propagation characteristics such as amplitude, speed, and attenuation.

Keywords: Micro-elongated; Refined Dual-Phase-Lag Model; Rotation; Fractional Conformable Derivative

Cite this article: Ramady A., Ismail M. F., Ahmed H. M., Alkhatib S., Ramadan E. M., El-Ganzoury E. N. S. Effect of Rotation on Wave Propagation in Micro-elongated Thermo-elastic Media with Fractional Conformable Derivative under the Refined Dual-Phase-Lag Model. Math. Sci 2026; *20*(1): 19-29 https://doi.org/10.57647/mathsci.2026.46781

List of Nomenclature

Quantity	Definition
$\mathbf{u}$	Displacement vector,
$\alpha_{t_1}, \alpha_{t_2}$	Coefficient of linear thermal expansion, where $\gamma_0 = (3\lambda + 3\mu)\,\alpha_{t_1}$, $\gamma_1 = (3\lambda + 3\mu)\,\alpha_{t_2}$,
λ and μ	Constants of Lame,
j^*	Microinertia,
T_0	Reference temperature,
Ω	Initial stress,
$\lambda_0, \lambda_1, a_0$	Constants of micro-elongational,

Quantity	Definition
ψ	Micro-elongational scalar,
Θ	Temperature,
c_e	Specific heat,
ρ	Density,
t	Time,
k	Thermal conductivity,
τ_θ	Phase-lag of the temperature gradient,
σ_{ij}	Component of stress tensor,
τ_q	Phase-lag of the heat flux.

1. Introduction

Micro-elongated thermo-elastic materials are part of a wider category of generalized continua that extend beyond the conventional deformation behavior of solids by incorporating additional micro-elongation affects. Unlike classical thermo-elastic theories, which describe mechanical behavior solely through displacement fields and thermal behavior via temperature variations, micro-elongated theories introduce an extra kinematic variable representing internal micro-level stretching. This internal elongation can correspond to phenomena such as fiber extension, molecular chain deformation, pore-structure distortion, or reorientation of microstructural elements within the material. By including this micro-elongation field, the thermo-mechanical response of complex materials such as composite media, biological tissues, polymeric substances, porous solids, and engineered microstructured materials can be described more comprehensively, as internal components are allowed to deform independently of the overall bulk motion. When coupled with thermal affects, micro-elongation interacts with the temperature field, generating additional stress contributions and heat transfer mechanisms that are absent in classical thermo-elastic models. Consequently, wave propagation, stress development, and temperature evolution in micro-elongated media exhibit distinctive features including attenuation, dispersion, and relaxation affects governed by the underlying microstructure (see [1, 2, 3, 4, 5, 6, 7, 8]). This theoretical approach is particularly valuable for analyzing dynamic phenomena, thermo-elastic interactions, and materials subjected to thermal loading, where delayed and spatially varying internal responses cannot be accurately captured by traditional thermo-elastic frameworks.

Fractional thermo-elasticity is an advanced generalization of classical thermo-elastic theories, incorporating fractional-order derivatives into the equation of energy. Within this framework, heat conduction is extended using fractional derivatives, allowing the model to capture non-Fourier heat transfer phenomena, such as finite-speed thermal wave propagation and dispersive affects. The inclusion of fractional parameters enhances the model's flexibility, improving the description of thermal lag, damping, wave attenuation, and dynamic stability in complex materials. As a result, fractional thermo-elasticity provides a more accurate and adaptable approach for analyzing modern engineering systems and advanced material structures, effectively representing behaviors that classical theories cannot fully capture. For further foundational studies on this subject, readers are referred to [9, 10, 11, 12, 13, 14, 15, 16, 17, 18, 19, 20].

The RDPL model introduces a sophisticated extension of heat conduction theories and serves as an improved version of the original DPL model. While the DPL model accounts for two distinct phase lags one associated with the temperature gradient and the other with the heat flux, it often falls short in capturing the complex thermal delay mechanisms that occur in real materials, particularly when they are subjected to rapid or high-intensity thermal excitations. These shortcomings become especially pronounced in scenarios involving ultrafast thermal processes, such as laser-induced heating, advanced micro-electronic cooling technologies, and the propagation of thermo-elastic waves, where heat transfer deviates significantly from the classical diffusive behavior. To overcome these limitations, the RDPL model represents more advanced features, including higher-order terms and carefully adjusted phase-lag parameters, which together provide a more refined representation of the thermal response. This enhanced structure allows the model to more accurately reflect the finite speed at which thermal disturbances propagate and to better represent the intrinsic properties of materials. Consequently, the RDPL model effectively describes thermal transport in regimes where heat does not spread instantaneously, but travels with a measurable delay, exhibiting characteristics similar to those of thermal waves. In addition to its improved physical accuracy, Comprehensive explanations, derivations, and theoretical insights into the RDPL model are available in references [21, 22, 23, 24, 25, 26, 27, 28, 29]. Because of its increased precision and stability, the RDPL model has become an important tool for analyzing thermo-elastic behavior in applications.

The influence of rotation on thermo-elasticity plays a crucial role in accurately describing the mechanical and thermal responses of solids subjected to high-speed or angular motion. When a thermo-elastic medium undergoes rotation, additional inertial forces, namely the Coriolis force, centrifugal force, and Euler acceleration become significant and modify the governing field equations. These rotational affects introduce coupling among the elastic and thermal fields and lead to substantial changes in wave propagation characteristics, stress and temperature. In rotating systems, the centrifugal force tends to stretch or compress the material depending on the angular velocity and radial position, resulting in modified equilibrium states and altered deformation patterns. Meanwhile, the Coriolis force influences the propagation of thermo-elastic waves, producing directional asymmetry and frequency shifts that are absent in non-rotating media. Furthermore, rotation can enhance or suppress thermal diffusion depending on the material constants and rotational speed, leading to non-uniform temperature fields and dynamic instabilities under certain conditions for more details, see [30, 31, 32,

33, 34, 35, 36, 37, 38]. Such affects become especially important in advanced engineering applications, including rotating machinery, spacecraft structures, turbine blades, micro-electromechanical devices, and geophysical models of the Earth's interior, where both rapid rotation and thermal loading coexist. Incorporating rotation into thermo-elastic theories allows for more realistic predictions of thermal stresses, wave speeds, damping behavior, and energy transport, ensuring the reliability and safety of structures operating in rotating environments.

Although thermo-elasticity has been widely studied using phase-lag models and fractional derivatives, and the mechanical behavior of micro-elongated materials has been investigated separately, a significant gap remains in the literature regarding their combined interaction within the fractional-order RDPL model. Most existing studies treat these affects independently, focusing either on fractional-order deformation or on non-Fourier heat conduction, while neglecting the simultaneous influence of micro-elongation and rotation. To date, no reported work has unified micro-elongated behavior, rotational affects, fractional derivatives, and the RDPL model within a single thermo-elastic formulation. Therefore, a primary objective of the present study is to fill this gap by developing a comprehensive model that captures the coupled thermo-mechanical and fractional-order responses of rotating micro-elongated materials under the RDPL model.

This paper investigates how rotation and fractional conformable derivatives affect the thermo-elastic behavior of a micro-elongated half-space within L-S theory, DPL model, and RDPL model. The governing equations for motion, heat conduction, and micro-elongation are first established and then rewritten in dimensionless form. Using Normal Mode Analysis, the system of partial differential equations is reduced to ordinary differential equations, and the boundary conditions at $z = 0$ are applied to determine the necessary solution constants. After obtaining the analytical solutions, numerical and graphical analyses are performed to study the affects of rotation and fractional parameters on displacement, stress fields, and micro-elongation. The results clearly show that both rotation and fractional-order affects significantly modify the thermo-micro-elongated response of the medium under the three considered models.

2. Governing equations

This section presents the principal governing equations that characterize the 2−dimensional micro-elongated thermo-elastic response as formulated within the frameworks of the L-S theory, the DPL model, and the RDPL model. Particular emphasis is placed on examining how rotational affects the behavior of the system. For the sake of mathematical convenience and to enable more effective analytical treatment, the governing relations are subsequently transformed into a nondimensional form.

The equation of motion can be expressed in the following form [39, 40]

$$\sigma_{ij,j} = \rho \left[u_{i,tt} + \{\mathbf{\Omega} \wedge (\mathbf{\Omega} \wedge \mathbf{u})\}_i + \left(2\mathbf{\Omega} \wedge \mathbf{u}_{,t}\right)_i \right], \quad (1)$$

where

$$\sigma_{ij} = 2\mu\varepsilon_{ij} + (\lambda e - \gamma_0\Theta + \lambda_0\psi)\,\delta_{ij}. \quad (2)$$

The equation of micro-elongation can be displayed in the following form [41]

$$a_0\psi_{,ii} + \gamma_1\Theta - \lambda_1\psi - \lambda_0 u_{j,j} = \frac{\rho j^*\psi_{,tt}}{2}. \quad (3)$$

The equation of energy can be written in the following form [23, 42]:

$$\begin{aligned} 0 \;=\; & k\left(1 + \Sigma_{n=1}^{N} \frac{\tau_\theta^{n-1+\alpha}}{\Gamma(n+\alpha)} \frac{\partial^\alpha}{\partial t^\alpha} \frac{\partial^{n-1}}{\partial t^{n-1}}\right)\Theta_{,ii} \quad (4)\\ & -\gamma_1 T_0 \psi_{,t} - \left(1 + \Sigma_{n=1}^{N} \frac{\tau_q^{n-1+\alpha}}{\Gamma(n+\alpha)} \frac{\partial^\alpha}{\partial t^\alpha} \frac{\partial^{n-1}}{\partial t^{n-1}}\right)\\ & \times \left[\gamma_0 T_0 \left(u_{,xt} + w_{,zt}\right) + \rho c_e \Theta_{,t}\right], \end{aligned}$$

where, $\frac{\partial^\alpha}{\partial t^\alpha}$ is the conformable fractional derivative of order $0 < \alpha \leq 1$ [43].

When
1- $N = 3$ and ($\tau_\theta < \tau_q \neq 0$, $k \neq 0$) is RDPL model,
2- $N = 1$ and ($\tau_\theta < \tau_q \neq 0$, $k \neq 0$) is DPL model,
3- $N = 1$ and ($\tau_\theta = 0$, $\tau_q \neq 0$, $k \neq 0$) is L-S theory.

Definition [44, 45]. Let f be a function such that $f : [a, \infty) \to \mathbb{R}$. Then, the conformable derivative of a function f is defined as

$$D_t^\alpha f(t) = \lim_{\epsilon \to 0} \frac{f\left(t + \epsilon t^{1-\alpha}\right) - f(t)}{\epsilon},$$

for all $t \geq a$, $\alpha \in (0, 1]$.

In the RDPL model formulation, setting N=3 introduces higher-order phase-lag terms that extend the classical DPL model and allow a more accurate description of heat conduction in microstructured materials. In Equation (4), the coupling term $(-\gamma_1 T_0 \psi_{,t})$ represents the direct interaction between the thermal field and the micro-elongation variable (ψ), indicating that the rate of micro-elongation contributes to the temperature evolution. The inclusion of higher-order terms enhances the model's capability to capture thermo–microstructural interactions and finite thermal wave propagation.

From Eq. (2) in Eq. (1) with the aid of the displacement vector $\mathbf{u}(x, z, t) = u(u, 0, w)$ and rotation Ω, we see

$$\begin{aligned} & \mu\nabla^2 u + (\lambda + \mu)\, e_{,x} - \gamma_0\Theta_{,x} + \lambda_0\psi_{,x} \quad (5)\\ & \quad = \rho\left[u_{,tt} - \Omega^2 u + 2\Omega w_{,t}\right], \end{aligned}$$

$$\begin{aligned} & \mu\nabla^2 w + (\lambda + \mu)\, e_{,z} - \gamma_0\Theta_{,z} + \lambda_0\psi_{,z} \quad (6)\\ & \quad = \rho\left[w_{,tt} - \Omega^2 w - 2\Omega u_{,t}\right]. \end{aligned}$$

10.57647/mathsci.2026.46781

Employing the displacement vector $\mathbf{u}(x,z,t) = u(u,0,w)$ in Eq. (3), we infer

$$a_0\psi_{,ii} + \gamma_1\Theta - \lambda_1\psi - \lambda_0\left(u_{,x} + w_{,z}\right) = \frac{\rho j^*\psi_{,tt}}{2}. \quad (7)$$

By applying the properties of the conformable derivative as outlined in [46] to Eq. (4), the equation takes the following form:

$$\begin{aligned} 0 &= k\left(1 + \Sigma_{n=1}^{N}\frac{\tau_\theta^{n-1+\alpha}}{\Gamma(n+\alpha)}\left(t^{1-\alpha}\right)\frac{\partial^n}{\partial t^n}\right)\Theta_{,ii} \quad (8)\\ &-\gamma_1 T_0\psi_{,t} - \left(1 + \Sigma_{n=1}^{N}\frac{\tau_q^{n-1+\alpha}}{\Gamma(n+\alpha)}\left(t^{1-\alpha}\right)\frac{\partial^n}{\partial t^n}\right)\\ &\times[\rho c_e\Theta_{,t} + \gamma_0 T_0(u_{,xt} + w_{,zt})]. \end{aligned}$$

In this analysis, we employ the following nondimensional variables to streamline the governing equations

$$\begin{aligned} (x,z) &= \frac{c_1}{\omega^*}(\bar{x},\bar{z}), \quad (9)\\ (u,v) &= \frac{T_0\gamma_0}{\rho c_1\omega^*}(\bar{u},\bar{v}),\\ \left(t,\tau_\theta,\tau_q\right) &= \frac{\left(\bar{t},\bar{\tau}_\theta,\bar{\tau}_q\right)}{\omega^*},\\ \Theta &= T_0\bar{\Theta}, \quad \sigma_{ij} = \gamma_1 T_0\bar{\sigma}_{ij},\\ \psi &= \frac{\gamma_0 T_0}{\lambda_0}\bar{\psi}, \quad \Omega = \omega^*\bar{\Omega},\\ k\omega^* &= \rho c_1^2 c_e, \quad \rho c_1^2 = \lambda + \mu. \end{aligned}$$

Utilizing Eq. (9) in Eqs. (5), (6), (7), and (8), one uncovers

$$\left(a_1\nabla^2 - \frac{\partial^2}{\partial t^2} + a_2\frac{\partial^2}{\partial x^2} + \Omega^2\right)u + \left(a_2\frac{\partial^2}{\partial x\partial z} - 2\Omega\frac{\partial}{\partial t}\right)w - \frac{\partial\Theta}{\partial x} + \frac{\partial\psi}{\partial x} = 0, \quad (10)$$

$$\left(a_2\frac{\partial^2}{\partial x\partial z} + 2\Omega\frac{\partial}{\partial t}\right)u + \left(a_1\nabla^2 - \frac{\partial^2}{\partial t^2} + a_2\frac{\partial^2}{\partial z^2} + \Omega^2\right)w - \frac{\partial\Theta}{\partial z} + \frac{\partial\psi}{\partial z} = 0, \quad (11)$$

$$a_5\frac{\partial u}{\partial x} + a_5\frac{\partial w}{\partial z} - a_3\Theta - \left(\nabla^2 - a_4 - a_6\frac{\partial^2}{\partial t^2}\right)\psi = 0, \quad (12)$$

$$a_8(1+\tau_2)\frac{\partial^2 u}{\partial x\partial t} + a_8(1+\tau_2)\frac{\partial^2 w}{\partial z\partial t} - \left(\nabla^2 + \tau_1\nabla^2 - a_7\frac{\partial}{\partial t} - \tau_2 a_7\frac{\partial}{\partial t}\right)\Theta + a_9\frac{\partial\psi}{\partial t} = 0, \quad (13)$$

where, $a_1 = \frac{\mu}{c_1^2\rho}$, $a_2 = \frac{\mu+\lambda}{c_1^2\rho}$, $a_3 = \frac{\lambda_0\gamma_1 c_1^2}{\gamma_0 a_0\omega^{*2}}$, $a_4 = \frac{c_1^2\lambda_1}{a_0\omega^{*2}}$, $a_5 = \frac{\lambda_0^2}{a_0\rho\omega^{*2}}$, $a_6 = \frac{\rho j^* c_1^2}{2a_0}$, $a_7 = \frac{\rho c_e c_1^2}{k\omega^*}$, $a_8 = \frac{\gamma_0^2 T_0}{k\omega^*\rho}$, $a_9 = \frac{\gamma_0\gamma_1 T_0 c_1^2}{k\omega^*\lambda_0}$, $\tau_1 = \Sigma_{n=1}^{N}\frac{i\omega\tau_\theta^{n-1+\alpha}}{\Gamma(n+\alpha)}\left(t^{1-\alpha}\right)\frac{\partial^n}{\partial t^n}$, and $\tau_2 = \Sigma_{n=1}^{N}\frac{i\omega\tau_q^{n-1+\alpha}}{\Gamma(n+\alpha)}\left(t^{1-\alpha}\right)\frac{\partial^n}{\partial t^n}$.

Employing Eq. (9) in Eq. (2), we obtain

$$\sigma_{xx} = \frac{\partial u}{\partial x} + a_{10}\frac{\partial w}{\partial z} - \Theta + \psi, \quad (14)$$

$$\sigma_{zz} = a_{10}\frac{\partial u}{\partial x} + \frac{\partial w}{\partial z} - \Theta + \psi, \quad (15)$$

$$\sigma_{zx} = \sigma_{xz} = a_1\frac{\partial u}{\partial z} + a_1\frac{\partial w}{\partial x}. \quad (16)$$

where, $a_{10} = \frac{\lambda_0^2}{a_0\rho\omega^{*2}}$.

The displacement potentials $\eta(x,z,t)$ and $\xi(x,z,t)$ which relate to displacement components have been introduced,we realize

$$u = \eta_{,x} + \xi_{,z}, \qquad w = \eta_{,z} - \xi_{,x}. \quad (17)$$

Using Eq. (17) in Eqs. (10), (11), (12), and (13), one obtains

$$\left[(a_1+a_2)\nabla^2 + \Omega^2 - \frac{\partial^2}{\partial t^2}\right]\eta + 2\Omega\xi_{,t} - \Theta + \psi = 0, \quad (18)$$

$$2\Omega\eta_{,t} - \left[a_1\nabla^2 + \Omega^2 - \frac{\partial^2}{\partial t^2}\right]\xi = 0, \quad (19)$$

$$a_5\nabla^2\eta - a_3\Theta - \left(\nabla^2 - a_4 - a_6\frac{\partial^2}{\partial t^2}\right)\psi = 0, \quad (20)$$

$$a_8(1+\tau_2)\nabla^2\left(\frac{\partial\eta}{\partial t}\right) - \left(\nabla^2 + \tau_1\nabla^2 - a_7\frac{\partial}{\partial t} - \tau_2 a_7\frac{\partial}{\partial t}\right)\Theta + a_9\frac{\partial\psi}{\partial t} = 0. \quad (21)$$

3. Solution

The solution of the physical field variables can be represented and examined using normal mode analysis as follows:

$$\begin{aligned} &\left[u, w, \Theta, \psi, \eta, \xi, \sigma_{ij}\right](x,z,t) \quad (22)\\ &= \left[\tilde{u}, \tilde{w}, \tilde{\Theta}, \tilde{\psi}, \tilde{\eta}, \tilde{\xi}, \tilde{\sigma}_{ij}\right](z)\, e^{i\left(-bx + \frac{\omega t^\alpha}{\alpha}\right)}. \end{aligned}$$

where, ω is the wave number and b is the frequency

Inserting Eq. (22) into Eqs. (10), (11), (12), and (13), we realize

$$\left(\varsigma_1 D^2 + \varsigma_2\right)\tilde{\eta} + \varsigma_3\tilde{\xi} - \tilde{\Theta} + \tilde{\psi} = 0, \quad (23)$$

$$\varsigma_3\tilde{\eta} - \left[a_1 D^2 + \varsigma_4\right]\tilde{\xi} = 0, \quad (24)$$

$$\left[a_5 D^2 - \varsigma_5\right]\tilde{\eta} - a_3\tilde{\Theta} - \left(D^2 + \varsigma_6\right)\tilde{\psi} = 0, \quad (25)$$

$$\left[\varsigma_7 D^2 - \varsigma_8\right]\tilde{\eta} - \left(\varsigma_9 D^2 - \varsigma_{10}\right)\tilde{\Theta} + \varsigma_{11}\tilde{\psi} = 0, \quad (26)$$

where, $\varsigma_1 = a_1 + a_2$, $\varsigma_2 = \omega^2 t^{2\alpha-2} - i(\alpha-1)\omega t^{\alpha-2} + \Omega^2 - b^2\varsigma_1$, $\varsigma_3 = 2i\Omega\omega t^{\alpha-1}$, $\varsigma_4 = \omega^2 t^{2\alpha-2} - i(\alpha-1)\omega t^{\alpha-2} + \Omega^2 - a_1 b^2$, $\varsigma_5 = b^2 a_5$, $\varsigma_6 = a_6\left[\omega^2 t^{2\alpha-2} - i(\alpha-1)\omega t^{\alpha-2}\right] - a_4 - b^2$, $\varsigma_7 = ia_8(1+\tau_2)\omega t^{\alpha-1}$, $\varsigma_8 = \varsigma_7 b^2$, $\varsigma_9 = (1+\tau_1)$, $\varsigma_{10} = \varsigma_9 b^2 + i(1+\tau_2)a_7\omega t^{\alpha-1}$, $\varsigma_{11} = ia_9\omega t^{\alpha-1}$.

It is observed that the cases

10.57647/mathsci.2026.46781

1. $\tau_1 = \frac{i\omega\tau_\theta^\alpha}{\Gamma(1+\alpha)} + \frac{\omega\tau_\theta^{1+\alpha}}{\Gamma(2+\alpha)}\left[it^{-1} - \omega t^{\alpha-1}\right] + \frac{\omega\tau_\theta^{2+\alpha}}{\Gamma(3+\alpha)}[i(\alpha-1)(\alpha-2)t^{-2} - 3\omega(\alpha-1)t^{\alpha-2} - i\omega^2 t^{2\alpha-2}]$ and
$\tau_2 = \frac{i\omega\tau_q^\alpha}{\Gamma(1+\alpha)} + \frac{\omega\tau_q^{1+\alpha}}{\Gamma(2+\alpha)}\left[it^{-1} - \omega t^{\alpha-1}\right] + \frac{\omega\tau_q^{2+\alpha}}{\Gamma(3+\alpha)}[i(\alpha-1)(\alpha-2)t^{-2} - 3\omega(\alpha-1)t^{\alpha-2} - i\omega^2 t^{2\alpha-2}]$ correspond to the RDPL model

2. $\tau_1 = \frac{i\omega\tau_\theta^\alpha}{\Gamma(\alpha+1)}$ and $\tau_2 = \frac{i\omega\tau_q^\alpha}{\Gamma(\alpha+1)}$ correspond to the DPL model

3. $\tau_1 = 0$ and $\tau_2 = \frac{i\omega\tau_q^\alpha}{\Gamma(\alpha+1)}$ correspond to the L-S theory

Equations (23), (25), and (26) yield a nontrivial solution when the determinant of the coefficient matrix associated with the physical quantities equals zero. Using the MATLAB program, one acquires

$$\left(D^8 - A_1D^6 + A_2D^4 - A_3D^2 + A_4\right)\{\tilde{\eta}(z), \tilde{\xi}(z), \tilde{\Theta}(z), \tilde{\psi}(z)\} = 0, \tag{27}$$

where, $A_1 = \frac{-1}{\varsigma_1\varsigma_9 a_1}\{-\varsigma_7 a_1 + \varsigma_9 a_1 a_5 + \varsigma_1\varsigma_4\varsigma_9 - \varsigma_1\varsigma_{10}a_1 + \varsigma_2\varsigma_9 a_1 + \varsigma_1\varsigma_6\varsigma_9 a_1\}$,
$A_2 = \frac{1}{\varsigma_1\varsigma_9 a_1}\{\varsigma_4\varsigma_7 + \varsigma_3^2\varsigma_9 - \varsigma_7 a_1 a_3 - \varsigma_{10}a_1 a_5 - \varsigma_{11}a_1 a_5 - \varsigma_1\varsigma_4\varsigma_{10} + \varsigma_2\varsigma_4\varsigma_9 - \varsigma_2\varsigma_{10}a_1 - \varsigma_6\varsigma_7 a_1 - \varsigma_5\varsigma_9 a_1 + \varsigma_4\varsigma_9 a_5 + \varsigma_1\varsigma_4\varsigma_6\varsigma_9 - \varsigma_1\varsigma_6\varsigma_{10}a_1 + \varsigma_2\varsigma_6\varsigma_9 a_1 + \varsigma_1\varsigma_{11}a_1 a_3 + \varsigma_8 a_1\}$,
$A_3 = \frac{-1}{\varsigma_1\varsigma_9 a_1}\{\varsigma_4\varsigma_8 + \varsigma_3^2\varsigma_6\varsigma_9 - \varsigma_2\varsigma_4\varsigma_{10} - \varsigma_4\varsigma_6\varsigma_7 - \varsigma_4\varsigma_5\varsigma_9 - \varsigma_4\varsigma_7 a_3 + \varsigma_6\varsigma_8 a_1 + \varsigma_5\varsigma_{10}a_1 + \varsigma_5\varsigma_{11}a_1 - \varsigma_4\varsigma_{10}a_5 - \varsigma_4\varsigma_{11}a_5 - \varsigma_1\varsigma_4\varsigma_6\varsigma_{10} + \varsigma_2\varsigma_4\varsigma_6\varsigma_9 + \varsigma_1\varsigma_4\varsigma_{11}a_3 - \varsigma_2\varsigma_6\varsigma_{10}a_1 + \varsigma_2\varsigma_{11}a_1 a_3 - \varsigma_3^2\varsigma_{10} + \varsigma_8 a_1 a_3\}$,
$A_4 = \frac{1}{\varsigma_1\varsigma_9 a_1}\{\varsigma_4\varsigma_6\varsigma_8 + \varsigma_4\varsigma_5\varsigma_{10} + \varsigma_4\varsigma_5\varsigma_{11} + \varsigma_4\varsigma_8 a_3 - \varsigma_3^2\varsigma_6\varsigma_{10} + \varsigma_3^2\varsigma_{11}a_3 - \varsigma_2\varsigma_4\varsigma_6\varsigma_{10} + \varsigma_2\varsigma_4\varsigma_{11}a_3\}$. This equation can be expressed as

$$\left(D^2 - r_1\right)\left(D^2 - r_2\right)\left(D^2 - r_3\right)\left(D^2 - r_4\right)\{\tilde{\eta}(z), \tilde{\xi}(z), \tilde{\Theta}(z), \tilde{\psi}(z)\} = 0, \tag{28}$$

where, r_1, r_2, r_3 and r_4 are roots

The general solution of Eq. (28) bound as $z \to \infty$ can be written as

$$\tilde{\eta}(z) = \Sigma_{m=1}^4 G_m e^{-r_m z}, \tag{29}$$
$$\tilde{\xi}(z) = \Sigma_{m=1}^4 \vartheta_{1m} G_m e^{-r_m z} \tag{30}$$
$$\tilde{\Theta}(z) = \Sigma_{m=1}^4 \vartheta_{2m} G_m e^{-r_m z}, \tag{31}$$
$$\tilde{\psi}(z) = \Sigma_{m=1}^4 \vartheta_{3m} G_m e^{-r_m z}. \tag{32}$$

where, $\vartheta_{1m} = \frac{\varsigma_3}{a_1 r_m^2 + \varsigma_4}$, $\vartheta_{2m} = \frac{\varsigma_7 r_m^4 + (\varsigma_6\varsigma_7 - \varsigma_8)r_m^2 - \varsigma_5\varsigma_{11} - \varsigma_6\varsigma_8}{\varsigma_9 r_m^4 + (\varsigma_6\varsigma_9 - \varsigma_{10})r_m^2 - \varsigma_6\varsigma_{10} - a_3\varsigma_{11}}$, and $\vartheta_{3m} = -\left(\varsigma_1 r_m^2 + \varsigma_2\right) - \varsigma_3\vartheta_{1m} + \vartheta_{2m}$.

Using Eq. (22) in Eq. (17), then employing Eqs. (29) and (30), one sees

$$\tilde{u} = -\Sigma_{m=1}^4 (r_m\vartheta_{1m} + ib) G_m e^{-r_m z}, \tag{33}$$
$$\tilde{w} = \Sigma_{m=1}^4 (ib\vartheta_{1m} - r_m) G_m e^{-r_m z}. \tag{34}$$

Utilizing Eq. (22) into Eqs. (14), (15), and (14), then using Eqs. (31), (32), (33) and (34), we infer

$$\tilde{\sigma}_{xx} = \Sigma_{m=1}^4 \vartheta_{4m} G_m e^{-r_m z}, \tag{35}$$
$$\tilde{\sigma}_{zz} = \Sigma_{m=1}^4 \vartheta_{5m} G_m e^{-r_m z}, \tag{36}$$
$$\tilde{\sigma}_{xz} = \tilde{\sigma}_{zx} = \Sigma_{m=1}^4 \vartheta_{6m} G_m e^{-r_m z}, \tag{37}$$

where, $\vartheta_{4m} = ib(1 - a_{10})r_m\vartheta_{1m} + a_{10}r_m^2 - b^2 - \vartheta_{2m} + \vartheta_{3m}$, $\vartheta_{5m} = ib(a_{10} - 1)r_m\vartheta_{1m} + r_m^2 - a_{10}b^2 - \vartheta_{2m} + \vartheta_{3m}$, $\vartheta_{6m} = a_1\left(r_m^2 + b^2\right)\vartheta_{1m} + 2iba_1 r_m$.

4. Boundary condition

To find the constants (G_1, G_2, G_3, and G_4), we have applied the boundary conditions for the problem at $z = 0$ as follows:

$$\sigma_{zz} = f_1 e^{i\left(-bx + \frac{\omega t^\alpha}{\alpha}\right)}, \tag{38}$$
$$\sigma_{xz} = 0,\ \Theta = f_2 e^{i\left(-bx + \frac{\omega t^\alpha}{\alpha}\right)},$$
$$\frac{\partial\psi}{\partial z} = 0,$$

where f_1 and f_2 are constants.

Mechanical boundary condition: When a mechanical force acts on the surface of the half-space, the boundary condition $\sigma_{zz} = f_1 e^{i\left(-bx + \frac{\omega t^\alpha}{\alpha}\right)}$ is applied. When the surface of the half-space is free of traction, the boundary condition $\sigma_{xz} = 0$ is used. $\Theta = f_2 e^{i\left(-bx + \frac{\omega t^\alpha}{\alpha}\right)}$ indicates that The temperature at the boundary is harmonically varying in space and time, with amplitude And the fourth boundary condition, $\frac{\partial\psi}{\partial z} = 0$, is a constraint on the rate of change of microelongation normal to the surface.

Substituting the assumed functional forms of the variables into the boundary conditions given in (38), yields a set of relations that the system parameters must satisfy. This procedure leads to a system of four linear equations. To evaluate the unknown constants (G_1, G_2, G_3, G_4) the system is solved using the inverse matrix technique as shown below:

$$\begin{bmatrix} G_1 \\ G_2 \\ G_3 \\ G_4 \end{bmatrix} = \begin{bmatrix} \vartheta_{51} & \vartheta_{52} & \vartheta_{53} & \vartheta_{54} \\ \vartheta_{61} & \vartheta_{62} & \vartheta_{63} & \vartheta_{64} \\ \vartheta_{21} & \vartheta_{22} & \vartheta_{23} & \vartheta_{24} \\ -r_1\vartheta_{31} & -r_2\vartheta_{32} & -r_3\vartheta_{33} & -r_4\vartheta_{34} \end{bmatrix}^{-1} \begin{bmatrix} f_1 \\ 0 \\ f_2 \\ 0 \end{bmatrix} \tag{39}$$

5. Numerical discussions and results

This section provides a set of graphical plots that illustrate the solutions in two-dimensional form. These visual results are essential for demonstrating the evolution of the various field variables, thereby deepening the understanding of their physical behavior and the qualitative trends inherent in the solutions. For numerical evaluation, aluminum–epoxy is chosen as the thermo-elastic material due to its well-documented thermal and mechanical properties, which make it a suitable and reliable choice for investigating thermo-elastic interactions. The material constants required for the analysis

are taken from reputable references, and the numerical values used in the computations are summarized in the following [47]

$$j^* = 0.196 \times 10^{-4}\ \mathrm{m}^2, \quad \lambda = 7.59 \times 10^{10}\ \frac{\mathrm{N}}{\mathrm{m}^2},$$
$$\rho = 2190\ \frac{\mathrm{kg}}{\mathrm{m}^3}, \quad \mu = 1.89 \times 10^{10}\ \frac{\mathrm{N}}{\mathrm{m}^2},$$
$$\gamma_0 = 0.50 \times 10^5\ \frac{\mathrm{N}}{\mathrm{m}^2.\mathrm{K}}, \quad \lambda_0 = 0.37 \times 10^{10}\ \frac{\mathrm{N}}{\mathrm{m}^2},$$
$$\gamma_1 = 0.50 \times 10^5\ \frac{\mathrm{N}}{\mathrm{m}^2.\mathrm{K}}, \quad c_e = 966\ \frac{\mathrm{J}}{\mathrm{kg.K}},$$
$$k = 252\ \frac{\mathrm{J}}{\mathrm{m.s.K}}, \quad T_0 = 293^\circ\ \mathrm{K},$$
$$\lambda_1 = 0.37 \times 10^{10}\ \frac{\mathrm{N}}{\mathrm{m}^2}, \quad a_0 = 0.61 \times 10^{-10}\ \frac{\mathrm{N}}{\mathrm{m}^2},$$
$$\tau_\theta = 0.6\ \mathrm{s}, \quad \tau_q = 0.9\ \mathrm{s}, \quad f_1 = 15, \quad f_2 = 10.$$

In this paper, the numerical evaluations of all physical quantities are performed at the nondimensional time $t = 0.2$ across the spatial domain $0 \le z \le 2$ and along the surface $x = 1.5$. The numerical technique employed in this work is used to examine and describe the behavior and variations of the physical quantities u, w, ψ, σ_{zz}, and σ_{xz}. The graphical representations illustrate the theoretical predictions based on the L-S theory, DPL model, and RDPL model providing a comparative understanding of their respective behaviors. Figure 1, Figure 2, Figure 3, Figure 4 and Figure 5 present a detailed comparative analysis of the L-S theory, DPL model, and RDPL model, highlighting the effect of rotation for a fractional-order parameter of $\alpha = 0.5$.Figure 1 illustrates the influence of rotation on the horizontal displacement component u for the L-S theory, DPL model, and RDPL model. The results reveal that rotational motion induces noticeable modifications in the displacement amplitude due to the combined action of centrifugal and Coriolis forces. A reduction in the magnitude of u is observed as rotation increases, with the RDPL model exhibiting the strongest damping behavior owing to its enhanced phase-lag structure. Figure 2 presents the impact of rotation on the vertical displacement component w. The results indicate that rotation alters the vertical wave profile by introducing additional inertial coupling. The displacement amplitude decreases with increasing rotation, highlighting the stabilizing effect of rotational forces. Among the models, the RDPL model produces the most attenuated response, whereas the L-S theory yields a comparatively higher amplitude. Figure 3 depicts the distribution of the micro-elongation field ψ under different rotational conditions. The figure illustrates that rotation significantly microstructural deformation within the material. The reduction in ψ amplitude clarifies that the effect of rotational inertia on internal micro-elongated phenomena, with the RDPL model capturing this behavior most effectively. Figure 4 clarifies the impact of rotation on the normal stress component σ_{zz}. It is noted that rotational motion alters the stress distribution significantly, increasing compressive and tensile variations. RDPL model predicts lower stress amplitudes, showing better damping, while L-S theory produces the highest wave amplitude due to weaker relaxation effects. Figure 5 shows the influence of rotation on tangential stress σ_{xz}. The tangential stress becomes more oscillatory and shifts in amplitude depending on the thermo-elastic model. RDPL model again displays the strongest attenuation, confirming its suitability for rotating systems. Figure 1 shows the variation of the field quantity under consideration with respect to the spatial coordinate, illustrating the influence of rotation and the fractional conformable derivative within the RDPL thermoelastic framework. The results demonstrate that rotation significantly modifies the wave amplitude and attenuation, while the fractional parameter controls the memory-dependent behavior of the micro-elongated thermoelastic response. The obtained results are compared with previously published studies. It is observed that the numerical trends illustrated in Figure 1, Figure 2, Figure 3, Figure 4, Figure 5 and Figure 6 are in close qualitative agreement with those reported in [41, 48] when the current model is reduced to their special cases by neglecting RDPL model and fractional-order effects. The remaining differences are attributed to the combined influence of rotation, micro-elongated behavior, and the fractional conformable RDPL model, demonstrating the extended capability and novelty of the present analysis.Figure 7, Figure 8, Figure 9, Figure 10, Figure 11 and Figure 12 are introduced to clarify and interpret the variation of the previously discussed physical quantities considering the effect of rotation ($\Omega = 2$) within the RDPL model. These graphical results present an in-depth depiction of how the quantities respond for three different values of the fractional order parameter, denoted by α. Figure 7 shows the effect of different fractional orders α on the horizontal displacement u. Increasing the fractional order enhances effects in heat conduction, which slows thermal diffusion and modifies the displacement amplitude. Lower α produces higher oscillations, indicating stronger relaxation effects. Figure 8 displays the influence of varying the fractional order α on the vertical displacement w. The results show that lower fractional orders intensify heat conduction, generating sharper gradients and larger oscillations in the displacement field. Conversely, higher α values lead to a more diffusive thermal response and reduced mechanical disturbance. Figure 9 depicts the effect of different fractional orders α on the micro-elongation field ψ. A clear increase in micro-elongation amplitude is observed for smaller α, indicating that fractional thermal behavior enhances internal micro-elongation effects. Higher fractional orders yield smoother and more attenuated, reflecting faster thermal relaxation. Figure 10 demonstrates the distribution of the normal stress σ_{zz} for several fractional orders α. The results show that decreasing α produces stronger stress concentrations and sharper oscillations due to intensified thermal lag. In contrast, higher fractional orders lead to more uniform stress distributions with reduced peak values. Figure 11 presents the ef-

fect of the fractional-order parameter α on the tangential stress σ_{xz}. Lower values of α amplify the tangential response and increase oscillatory behavior, highlighting the thermal-mechanical coupling. As α increases, the tangential stresses become smoother and exhibit reduced amplitude. Figure 12 shows the effect of varying the fractional order α on the temperature Θ. The results show that lower fractional orders intensify heat conduction, generating sharper gradients and larger oscillations in the temperature. Conversely, higher α values lead to a more diffusive thermal response.

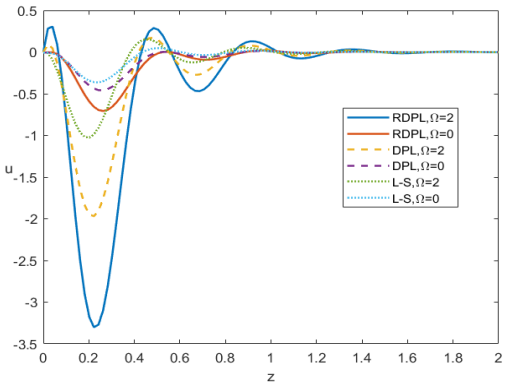

Figure 1. Impact of rotation on u.

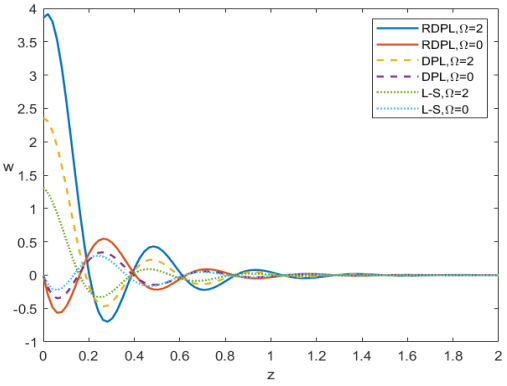

Figure 2. Impact of rotation on w.

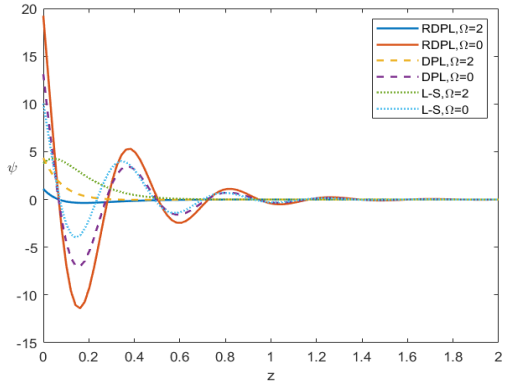

Figure 3. Impact of rotation on ψ.

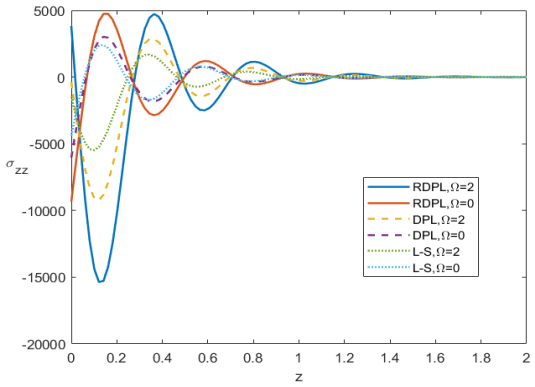

Figure 4. Impact of rotation on σ_{zz}.

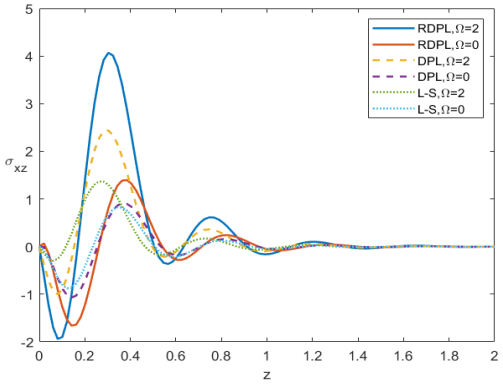

Figure 5. Impact of rotation on σ_{xz}.

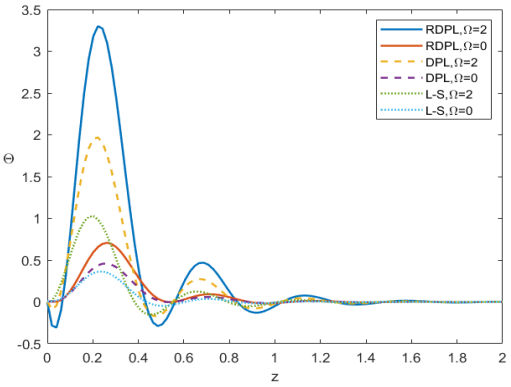

Figure 6. Impact of rotation on Θ.

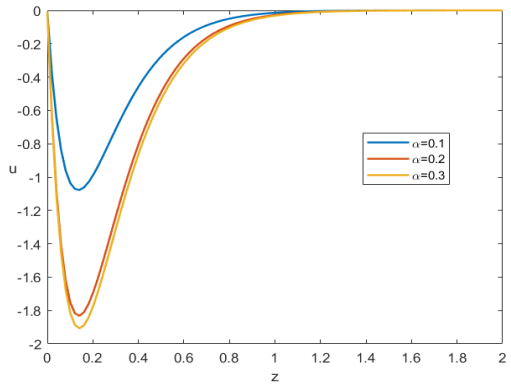

Figure 7. Effect of different fractional order (α) on u.

10.57647/mathsci.2026.46781

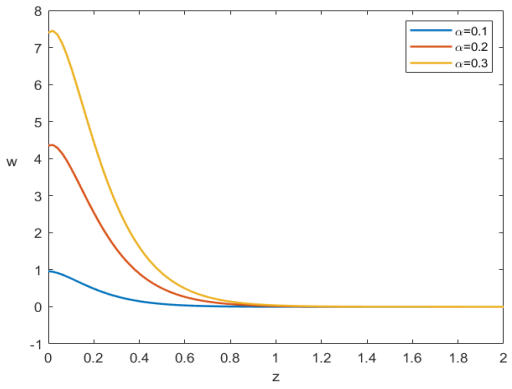

Figure 8. Effect of different fractional order (α) on w.

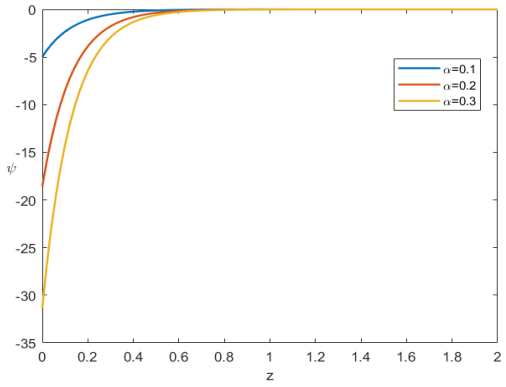

Figure 9. Effect of different fractional order (α) on ψ.

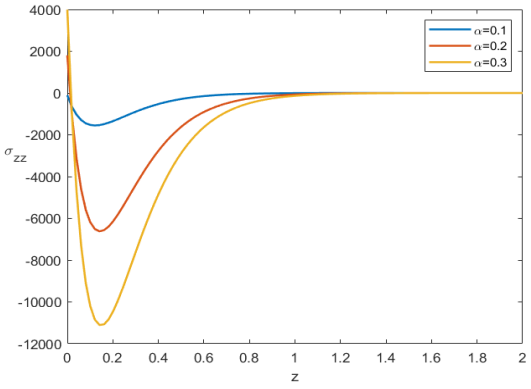

Figure 10. Effect of different fractional order (α) on σ_{zz}.

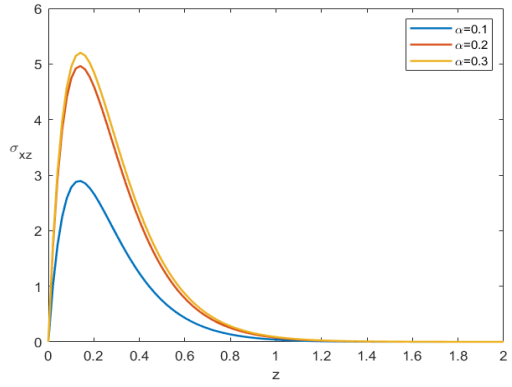

Figure 11. Effect of different fractional order (α) on σ_{xz}.

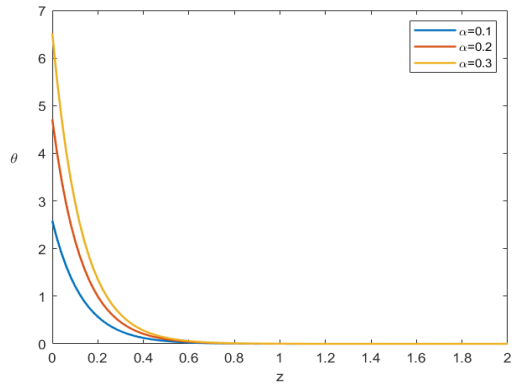

Figure 12. Effect of different fractional order (α) on Θ.

6. Conclusion

In this paper, the thermo-elastic response of a rotating micro-elongated half-space has been thoroughly investigated within the frameworks of the L-S theory, the DPL model, and the RDPL model, incorporating the effect of fractional conformable derivatives. The governing equations describing displacement, micro-elongation, and thermal fields were formulated, non-dimensionalized, and solved analytically using a normal mode approach. This allowed explicit solutions for all primary field variables to be obtained, facilitating a comprehensive investigation of wave propagation under rotation. The present results provide important insights into the behavior of rotating microstructured materials subjected to thermal loading. Such materials are commonly encountered in advanced composite components used in turbines, rotating machinery, and aerospace structures, where rotation-induced effects significantly influence thermo-elastic wave propagation and heat transfer characteristics. Rotation introduces additional inertial effects primarily the Coriolis and centrifugal forces which alter wave amplitude, propagation speed, and attenuation characteristics. These effects are particularly evident in the displacement fields, where both horizontal and vertical components experience noticeable modulation in response to increasing rotational speed. The micro-elongation field ψ is likewise strongly influenced by rotation, with its amplitude decreasing as rotational effects intensify, reflecting the inhibitory action of inertial forces on microstructural deformation. The stress components σ_{zz} and σ_{xz} exhibit distinct changes in magnitude and spatial distribution, illustrating how rotation enhances tangential stress interaction and alters normal stress oscillations within the medium. A comparative assessment among L-S theory, DPL model, and RDPL model reveals that the RDPL model consistently provides a more attenuated and physically realistic response due to its refined phase-lag formulation. This model proves especially effective in capturing the combined effects of fractional heat conduction, micro-elongation, and rotation.

The present analysis can be extended in several important directions. Future studies may consider two- and

10.57647/mathsci.2026.46781

three-dimensional configurations and more realistic geometries to better represent practical engineering structures. The influence of variable rotational speed, initial stress, magnetic fields, or poroplastic effects may also be incorporated to further enrich the physical model. In addition, comparing the fractional conformable derivative with other fractional operators could provide deeper insight into thermo-elastic behavior.

Acknowledgment

The project was funded by KAU Endowment (WAQF) at King Abdulaziz University, Jeddah, Saudi Arabia. The authors, therefore, acknowledge with thanks WAQF and the Deanship of Scientific Research (DSR) for technical and financial support.

Authors contributions

All the authors have participated sufficiently in the intellectual content, conception and design of this work or the analysis and interpretation of the data (when applicable), as well as the writing of the manuscript.

Availability of data and materials

The datasets used and/or analyzed during the current study are available from the corresponding author upon reasonable request.

Conflict of interests

The authors declare that they have no competing interests.

References

1. Ailawalia P, Sachdeva SK, and Pathania DS. Plane strain deformation in a thermoelastic microelongated solid with internal heat source. International Journal of Applied Mechanics and Engineering 2015; 20
2. Lotfy K. Thermo-mechanical waves of excited microelongated semiconductor layer during photothermal transport processes. Waves in Random and Complex Media 2022 :1–17
3. Hilal MI. Thermomechanical interactions of rotating thermoelastic magneto-microelongated medium heated by laser and initially stressed via non-local elasticity and GN III. Acta Mechanica 2022; 233:5183–97
4. El-Sapa S, Alhejaili W, Lotfy K, and El-Bary AA. Response of excited microelongated non-local semiconductor layer thermomechanical waves to photothermal transport processes. Acta Mechanica 2023; 234:2373–88
5. Alshehri AM, Lotfy K, and Ibrahim E. A novel model of microelongation thermomechanical photoacoustic waves in excited semiconductor materials. Results in Physics 2024; 63:107881
6. Kadian P, Kumar S, Hooda N, and Sangwan M. Reflection of plane waves in a non-local viscothermoelastic half-space under variable thermal conductivity and microelongation effects. Journal of Thermal Stresses 2024; 47:1479–99
7. Kadian P, Kumar S, and Sangwan M. Effect of inclined mechanical load on a rotating microelongated two temperature thermoelastic half space with temperature dependent properties. Journal of Vibration Engineering and Technologies 2024; 12:4053–74
8. Yadav K, Sheoran D, and Kalkal KK. Reflection of plane waves in a microelongated thermoelastic porous medium with Hall current under modified Green–Lindsay model. Acta Mechanica 2025; 236:1359–80
9. El-Karamany AS and Ezzat MA. On fractional thermoelasticity. Mathematics and Mechanics of Solids 2011; 16:334–46
10. Sumelka W. Thermoelasticity in the framework of the fractional continuum mechanics. Journal of Thermal Stresses 2014; 37:678–706
11. Ezzat M and Ezzat S. Fractional thermoelasticity applications for porous asphaltic materials. Petroleum Science 2016; 13:550–60
12. Sheoran SS and Kundu P. Fractional order generalized thermoelasticity theories: A review. International Journal of Advances in Applied Mathematics and Mechanics 2016; 3:76–81
13. Youssef HM. Theory of generalized thermoelasticity with fractional order strain. Journal of Vibration and Control 2016; 22:3840–57
14. Yu YJ and Deng ZC. Fractional order theory of Cattaneo-type thermoelasticity using new fractional derivatives. Applied Mathematical Modelling 2020; 87:731–51
15. Sherief HH and Hussein EM. Fractional order model of micropolar thermoelasticity and 2D half-space problem. Acta Mechanica 2023; 234:535–52
16. Mishra AK, Verma L, Nikan O, and Molavi-Arabshahi M. Numerical pricing of European options under time-fractional Black–Scholes equation in financial markets. Chaos: An Interdisciplinary Journal of Nonlinear Science 2025; 35
17. Prajapati VJ and Meher R. Solution of time-fractional Rosenau-Hyman model using a robust homotopy approach via formable transform. Iranian Journal of Science and Technology, Transactions A: Science 2022; 46:1431–44

18. Nikan O, Rashidinia J, and Jafari H. Numerically pricing American and European options using a time fractional Black–Scholes model in financial decision-making. Alexandria Engineering Journal 2025; 112:235–45
19. Javadi R, Mesgarani H, Nikan O, and Avazzadeh Z. Solving fractional order differential equations by using fractional radial basis function neural network. Symmetry 2023; 15:1275
20. Qiu W, Nikan O, and Avazzadeh Z. Numerical investigation of generalized tempered-type integrodifferential equations with respect to another function. Fractional Calculus and Applied Analysis 2023; 26:2580–601
21. Zenkour AM. Thermo-diffusion of solid cylinders based upon refined dual-phase-lag models. Multidiscipline Modeling in Materials and Structures 2020; 16:1417–34
22. Khamis AK, El-Bary AA, Lotfy K, and Bakali A. Photothermal excitation processes with refined multi dual phase-lags theory for semiconductor elastic medium. Alexandria Engineering Journal 2020; 59:1–9
23. Abouelregal AE. Modified fractional thermoelasticity model with multi-relaxation times of higher order: application to spherical cavity exposed to a harmonic varying heat. Waves in Random and Complex Media 2021; 31:812–32
24. Kutbi MA and Zenkour AM. Refined dual-phase-lag Green–Naghdi models for thermoelastic diffusion in an infinite medium. Waves in Random and Complex Media 2022; 32:947–67
25. Jeyaraman P, Mahesh S, Selvamani R, Dimitri R, and Tornabene F. Multi thermal waves in a thermo diffusive piezoelectric functionally graded rod via refined multi-dual phase-lag model. Curved and Layered Structures 2022; 9:105–15
26. Zenkour AM, Saeed T, and Aati AM. Refined dual-phase-lag theory for the 1D behavior of skin tissue under ramp-type heating. Materials 2023; 16:2421
27. De A, Purkait P, Das P, and Kanoria M. Memory dependent magneto-thermoelastic interaction in a rotating medium based on refined multi-phase-lag model. 2024. In press
28. Bhattacharya D and Kanoria M. Refined four-phase lag model for elasto-thermodiffusive interaction with harmonically varying heat sources. Mechanics of Time-Dependent Materials 2024; 28:1853–72
29. Hafed ZS, Abo-Dahab SM, Kilany AA, and Ahmed SE. Electromagnetic field on a photothermal semiconducting voids medium under Lord–Shulman and refined multi-phase lag models in thermoelasticity. International Journal of Modern Physics B 2025; 39:2550007
30. Rabie WB, Ahmed HM, Marin M, and Ismail MF. Exact Wave Solutions for Rotational Effects in Temperature-Dependent Thermoelastic Materials via IMETF Technique. Iranian Journal of Science and Technology, Transactions of Mechanical Engineering 2025 :1–28
31. Abd-Alla AM, Abo-Dahab SM, and Alsharif A. Thermal shock behaviour on generalized thermoelastic medium under initial stress with rotation. Mechanics of Solids 2024; 59:2861–75
32. Makkad G, Khalsa L, Abouelregal A, and Varghese V. Analysis of magneto-thermoviscoelastic behavior in rotating thermal-infused nanorods: exploring thermomass dynamics and Klein–Gordon nonlocality effects. Acta Mechanica 2025 :1–25
33. Abo-Dahab SM, Jaradat EK, Gafel HS, and Elidy ES. Rotational Influence on Wave Propagation in Semiconductor Nanostructure Thermoelastic Solid with Ramp-Type Heat Source and Two-Temperature Theory. Axioms 2025; 14:560
34. Alsaeed SS and Abouelregal AE. Advanced thermoelastic analysis of rotating nanobeams with temperature-dependent properties: incorporating non-local effects, size dependence, and thermal conduction models. Mechanics Based Design of Structures and Machines 2025 :1–29
35. Abouelregal AE, Askar SS, Marin M, and Mohamed B. The theory of thermoelasticity with a memory-dependent dynamic response for a thermo-piezoelectric functionally graded rotating rod. Scientific Reports 2023; 13:9052
36. Salah DM, Abd-Alla AM, and El-Kabeir SMM. Magneto-Thermoelastic Response of a Rotating Medium with Double Porosity under Initial Stress. Mechanics of Solids 2025 :1–19
37. Wang H, He T, and Ma Y. Investigation on the electro-magneto-thermoviscoelastic response of multilayer rotating hollow cylinder based on two-temperature theory and fractional-order viscoelastic systems. Mechanics of Advanced Materials and Structures 2025; 32:4196–224
38. Lotfy K, El-Bary A, and Elidy E. Magneto-photothermoelastic excitation rotating semiconductor medium based on moisture diffusivity. Computer Modeling in Engineering and Sciences 2024; 141:107
39. Rabie WB, Ahmed HM, Marin M, and Ismail MF. Exact Wave Solutions for Rotational Effects in Temperature-Dependent Thermoelastic Materials via IMETF Technique. Iranian Journal of Science and Technology, Transactions of Mechanical Engineering 2025 :1–28

40. Ismail MF, Ahmed HM, Marei GA, and Samir I. Comprehensive Analysis of Exact Wave Solutions in Temperature-Dependent Coupled Nonlinear Thermoelasticity Theory Using Advanced Analytic Methods. Journal of Vibration Engineering and Technologies 2025; 13:265
41. Othman MIA, Eraki EE, and Ismail MF. Study of micro-elongated thermoelastic medium loaded with a piezoelectric layer under the influence of gravity using the dual-phase-lag model. International Journal of Mechanical System Dynamics 2023; 3:136–45
42. Ismail MF, Ahmed HM, El-Bary AA, Youssef HM, and Samir I. Exploration of exact wave solutions for the Lord-Shulman thermo-elasticity theory with temperature dependence using advanced techniques. AIMS Mathematics 2025; 10:10806–30
43. Soliman M, Ahmed HM, Badra N, Nofal TA, and Samir I. Highly dispersive gap solitons for conformable fractional model in optical fibers with dispersive reflectivity solutions using the modified extended direct algebraic method. AIMS Mathematics 2024; 9:25205–22
44. Ghayad MS, Ahmed HM, Badra NM, Rezazadeh H, Hosseinzadeh MA, and Rabie WB. Extraction of new optical solitons of conformable time fractional generalized RKL equation via quadrupled power-law of self-phase modulation. Optical and Quantum Electronics 2024; 56:1304
45. Zhao D and Luo M. General conformable fractional derivative and its physical interpretation. Calcolo 2017; 54:903–17
46. Ullah N, Asjad MI, Awrejcewicz J, Muhammad T, and Baleanu D. On soliton solutions of fractional-order nonlinear model appears in physical sciences. AIMS Mathematics 2022; 7:7421–40
47. Othman MIA and Ismail MF. The gravitational field effect on a micro-elongated thermoelastic layer under a fluid load with two theories. Multidiscipline Modeling in Materials and Structures 2022; 18:757–71
48. Othman MIA, Eraki EE, and Ismail MF. Impact of rotation on a micro-elongated thermoelastic solid subjected to a load from an overlying liquid layer according to various theories. Physica Scripta 2024; 99:105214